



Technical Note: Real-time 3D MRI in the presence of motion for MRI-guided radiotherapy: 3D Dynamic keyhole imaging with super-resolution

Taeho Kim^{a)}, and Justin C. Park

Department of Radiation Oncology, Washington University School of Medicine, St Louis, MO 63110, USA

H. Michael Gach

Department of Radiation Oncology, Washington University School of Medicine, St Louis, MO 63110, USA

Department of Radiology and Biomedical Engineering, Washington University in St. Louis, St Louis, MO 63110, USA

Jaehee Chun

Department of Radiation Oncology, Yonsei University College of Medicine, Seoul 03722, South Korea

Sasa Mutic

Department of Radiation Oncology, Washington University School of Medicine, St Louis, MO 63110, USA

(Received 22 April 2019; revised 21 June 2019; accepted for publication 22 July 2019; published 27 August 2019)

Purpose: The purpose of this study was to present real-time three-dimensional (3D) magnetic resonance imaging (MRI) in the presence of motion for MRI-guided radiotherapy (MRgRT) using dynamic keyhole imaging for high-temporal acquisition and super-resolution generative (SRG) model for high-spatial reconstruction.

Method: We propose a unique real-time 3D MRI technique by combining a data sharing technique (3D dynamic keyhole imaging) with a SRG model using cascaded deep learning technique. 3D dynamic keyhole imaging utilizes the data sharing mechanism by combining keyhole central k-space data acquired in real-time with high-spatial, high-temporal resolution prior peripheral k-space data at various motion positions prepared by the SRG model. The efficacy of the 3D dynamic keyhole imaging with super-resolution (SR_dKeyhole) was compared to the ground-truth super-resolution images with the original full k-space data. It was also compared with the zero-filling reconstruction (zero-filling), conventional keyhole reconstruction with low-spatial high-temporal prior data (LR_cKeyhole), and conventional keyhole reconstruction with super-resolution prior data (SR_cKeyhole).

Results: High-spatial, high-temporal resolution 3D MRI datasets ($1.5 \times 1.5 \times 6 \text{ mm}^3$) were generated from low-spatial, high-temporal resolution 3D MRI datasets ($6 \times 6 \times 6 \text{ mm}^3$) using the cascaded deep learning SRG framework (<100 ms/volume). 3D dynamic keyhole imaging with the SRG model provided high-spatial, high-temporal resolution images ($1.5 \times 1.5 \times 6 \text{ mm}^3$, 455 ms) with the highest similarity to the ground-truth SR images without any noticeable artifacts. Structural similarity indices (SSIM) of the reconstructed 3D MRI to the original SR 3D MRI were 0.65, 0.66, 0.86, and 0.89 for zero-filling, LR_cKeyhole, SR_cKeyhole, and SR_dKeyhole, respectively (1 for identical image). In addition, average value of image relative error (IRE) of the reconstructed 3D MRI to the original SR 3D MRI were 0.169, 0.191, 0.079, and 0.067 for zero-filling, LR_cKeyhole, SR_cKeyhole, and SR_dKeyhole, respectively (0 for identical image).

Conclusions: We demonstrated that high-spatial, high-temporal resolution 3D MRI was feasible by combining 3D dynamic keyhole imaging with a SRG model in terms of image quality and imaging time. The proposed technique can be utilized for real-time 3D MRgRT. © 2019 American Association of Physicists in Medicine [https://doi.org/10.1002/mp.13748]

Key words: dynamic keyhole, integrated MRI and radiotherapy system, real-time 3D MRI, super-resolution

1. INTRODUCTION

Integrated magnetic resonance imaging (MRI) and radiotherapy systems are clinically established in image-guided radiotherapy (IGRT).^{1–4} Furthermore, there are several systems with unique configurations such as inline orientation with biplanar magnet and inline/perpendicular orientation with open magnet under development.^{5–8} The integrated MRI and radiotherapy systems can provide real-time tumor tracking, inclusive of changes in tumor position and

shape,^{2,9,10} since MRI produces superior soft tissue contrast of patient anatomy without ionizing radiation. MRI-guided radiotherapy (MRgRT) gives excellent local control with little toxicity.^{11,12}

Respiratory-related tumor motion can be detected using time-resolved 4D MRI and cine MRI.^{13–16} Time-resolved 4D MRI provides high-spatial resolution 3D MRI datasets with multiple respiratory amplitudes/phases. For example, in motion studies, iterative reconstruction techniques in 4D MRI improved image quality while reducing motion

artifacts.^{17–19} However, long acquisition and retrospective reconstruction times (>1 min) preclude their use for real-time tumor tracking in MRgRT. In addition, several real-time 3D MRI techniques were proposed with undersampled acquisition schemes,^{20,21} but their long reconstruction times are not suitable for real-time MRgRT. Near real-time 2D cine MRI with frame rates (~ 5 frames/sec) is currently utilized in real-time MRgRT and the acquired spatial resolution has been compromised (0.35×0.35 cm²).² However, tumors near the diaphragm showed 3D motion, reaching up to a 5 cm in range²² and rotating up to 45° ²³ during respiration.^{22,24} Therefore, high-spatial, high-temporal resolution 3D MRI is highly needed in real-time MRgRT.

One of the high-temporal resolution 3D MRI approaches for real-time tumor tracking is a data sharing technique. In conventional data sharing techniques such as keyhole imaging, high-temporal resolution is accomplished by reducing

the amount of temporal k-space data acquired in real-time (called keyhole data) and high-spatial resolution imaging is achieved by utilizing prior peripheral k-space data in conventional Fourier transform image reconstruction.²⁵ By utilizing anatomical motion information such as respiratory displacement in keyhole imaging, real-time 2D MRI in the presence of respiratory motion (i.e., dynamic keyhole imaging) can be acquired without noticeable motion artifacts.^{26,27} The previous studies demonstrated that the dynamic keyhole 2D cine imaging provided accurate tumor motion quantification with higher frame rates (~ 15 frames/sec),²⁶ implying a promising technique for real-time 3D cine MRI. However, high-spatial resolution 3D dynamic keyhole imaging has been challenged, since the spatial resolution of the temporal images is determined by the spatial resolution of the prior data in the dynamic keyhole imaging in Fig. 1. In [Fig. 1(b)], high-spatial resolution prior data with low-temporal resolution can be

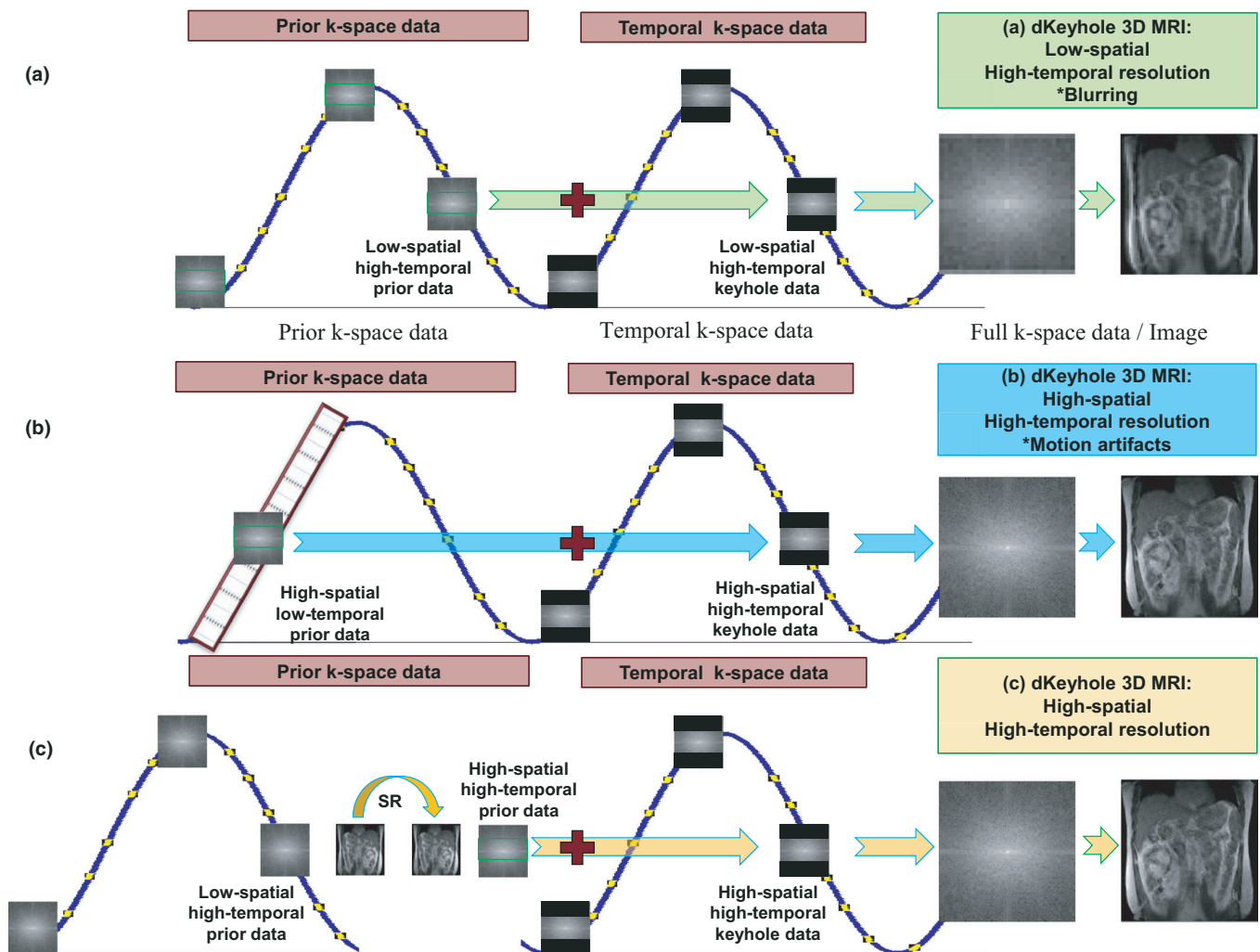


FIG. 1. Schematic of dynamic keyhole imaging for 3D MRI. In conventional 3D dynamic keyhole imaging in the presence of motion, (a) low-spatial, high-temporal resolution imaging is acquired (combining keyhole central k-space data in temporal data with peripheral k-space data in prior data). Since the spatial resolution of the temporal images is determined by the spatial resolution of the prior data in the dynamic keyhole imaging, (b) high-spatial, low-temporal resolution prior data cause motion artifacts in reconstructed high-spatial, high-temporal resolution 3D images. (c) high-spatial, high-temporal prior data generated from low-spatial, high-temporal prior data by deep learning is used for the high-spatial, high-temporal 3D dynamic keyhole imaging. [Color figure can be viewed at wileyonlinelibrary.com]

used in the reconstruction, but substantial blurring motion artifacts will degrade image quality. Therefore, the high-spatial, low-temporal resolution 3D prior data approach underperforms high-spatial, high-temporal resolution 3D imaging.

Recently, several super-resolution approaches have been introduced to MRI.^{28,29} As post-processing means, they can generate images with high-SNR and high-spatial resolution within a reasonable processing time frame from low-SNR and low-spatial images obtained with high frame rates.²⁹ Utilizing super-resolution can overcome a spatial resolution limitation in 3D dynamic keyhole imaging. The aim of this paper is to propose high spatial and temporal resolution 3D MRIs in the presence of motion for real-time 3D MRgRT by combining 3D dynamic keyhole imaging with super-resolution generative (SRG) model.

2. METHODS

The proposed techniques utilized two key components for high-spatial, high-temporal 3D MRI: (a) dynamic keyhole imaging for high-temporal acquisition; and (b) SRG model for high-spatial reconstruction.

2.A. Low-spatial, high-temporal resolution image acquisition

All data used in this study were acquired from a 0.35 T MRgRT system (ViewRay Inc., Oakwood Village, Ohio) with a three head Co-60 radiation therapy delivery system. MRIs of human subjects were acquired using anterior and posterior torso phased array receive only coils. Twenty real-time volumetric 3D MRI datasets were acquired continuously (free breathing) across multiple respiratory cycles for four human subjects. 3D images in coronal orientation were acquired using the true fast imaging using steady-state precession (TrueFISP). The generalized auto calibrating partially parallel acquisition (GRAPPA) technique was used to speed up image acquisition (iPAT = 2). Imaging parameters are base resolution = 64, phase partial Fourier = 6/8, TR/TE = 1.75/0.81 ms, voxel size = $6 \times 6 \times 6 \text{ mm}^3$, and total acquisition time/volume = 420 ms.

2.B. High-spatial, high-temporal resolution prior image generation (Super Resolution) using Cascaded deep learning

The deep learning (DL)-based SR generative (SRG) model for MRI accomplishes a significant improvement in spatial resolution compared to conventional SR techniques such as interpolation-based methods.³⁰ SR images can be generated without transformation models since DL-based methods utilize direct mapping based on information extracted from previous datasets. Recent studies have shown that the in-plane resolution of physically scanned low-spatial resolution 3D MRI can be improved to a four times higher resolution without compromising the image quality.²⁹

A cascaded DL-based SRG model used a splitting SR generation process to make a SR model robust compared to the conventional DL-based methods. The cascaded DL-based SR consisted of three training stages: (a) training of a denoising autoencoder (DAE) using noise reduced low-spatial resolution data; (b) training of a downsampling network (DSN) using a paired low-spatial resolution (LR)/high-spatial resolution (HR) data that allows the generation of perfectly paired LR/HR data from the clinically abundant HR scans; and (c) the training of a SRG trained with data generated by the DSN that maps from LR inputs to HR outputs. The training was performed using a GeForce GTX 1080 Ti GPU (NVIDIA, Santa Clara, CA).

1. Training of a denoising autoencoder (DAE): Image denoising is critical since SR generation suffers from image noise. Conventional image denoising techniques are not efficient in processing time and computation power. In the training process, we used a convolutional neural network (CNN)-based DAE for high accuracy. The DAE was trained with pairs of noisy and denoised LR MRIs that were preprocessed using the nonlocal means filter (NLM). Four hundred and eighty LR breath-hold images were used in the DAE training (training time: around 35 min).
2. Training of a downsampling network (DSN): After the DAE training, paired LR and HR MR images were used in the downsampling network training. The images were scanned from a phantom and volunteers in a single breath-hold. We manually selected the data pairs until the HR and LR scans were perfectly paired. We designed a CNN-based DSN for the downsampling process using 480 data pairs of LR and HR images. In the training, we ensured that the resulting LR images were similar to the ground-truth LR images from the scanner. HR MR images of 256×256 pixels ($1.5 \times 1.5 \text{ mm}^2$) and the corresponding LR images of 64×64 pixels ($6.0 \times 6.0 \text{ mm}^2$) were used in the testing and inferencing steps (training time: around 20 min).
3. Training of SRG model: The robustness of the DSN was a key component in the performance of the SRG model because the DSN was used to generate LR MRIs for the SRG model training. The SRG network was then trained with 4,475 data pairs from the set of axial LR MRIs to create axial SR MRIs and 1,375 data pairs from LR 4D MRIs to create SR 4D MRIs, respectively. The data pairs consisted of clinically available HR MR images and the corresponding LR images generated by the DSN. In the training, we verified the SRG model with fast axial MRI in a breath-hold and multivolumetric cine 3D MRI. The axial SR MRIs were generated from the set of axial LR MRIs acquired in a short breath-hold interval (<3 s). SR multivolumetric cine 3D MRIs were generated from multivolumetric LR cine 3D MRI acquired at rate of 2 volumes/sec (training time: around 4 h 15 min).

After the verification of DL-based SRG model, we generated the SR multivolumetric cine 3D MRIs from LR MRIs using the SRG model (20 SR volumetric cine 3D MRI datasets/each human subject). In this study, we utilized the pairs of the SR multivolumetric cine 3D MRI and the LR multivolumetric cine 3D MRI. The SR MRIs were used as the ground-truth images for the comparison study.

2.C. 3D dynamic keyhole imaging with a library of the prior data

Figure 1 shows the scheme of the 3D dynamic keyhole imaging. The dynamic keyhole imaging uses a library of prior peripheral k-space data in combination with keyhole k-space data acquired in real-time. For high-spatial, high-temporal 3D dynamic keyhole imaging, high spatial and temporal resolution prior k-space data at various respiratory positions were needed as a library of the prior data in 3D dynamic keyhole imaging.

Twenty real-time volumetric 3D MRI datasets from each of four human subject were used in the comparison study. Each dataset included low-spatial, high-temporal resolution images from the acquisition and high-spatial, high-temporal resolution images generated using the SRG model. Respiratory displacement was extracted from the profile of the diaphragm on the coronal middle slice of the high-spatial, high-temporal resolution 3D MRI. Based on each subject's respiratory patterns, approximately ten respiratory positions were sampled through a couple of respiratory cycles. The corresponding high-spatial high-temporal resolution MRI datasets were used as the prior data associated with the respiratory position. The remaining high-spatial, high-temporal resolution MRI datasets were used as the temporal data in the 3D dynamic keyhole imaging.

In the simulation studies, all SR image data were Fourier transformed into k-space. Approximately ten volumetric SR MR k-space datasets were used as the prior k-space dataset and the remaining volumetric SR MR k-space datasets were used as the temporal k-space datasets. The size of the keyhole k-space data was empirically determined in consideration of image quality and time. The k-space data matrix ($k_x \times k_y \times k_z$) was $256 \times 256 \times 10$. The size of keyhole k-space data was 26 k_y lines/slice. The size of the prior peripheral k-space data was 230 k_y lines/slice. The prior peripheral and keyhole k-space data were matched based on respiratory displacements to accelerate acquisition time and improve image quality in the presence of motion.²⁶ Images were reconstructed using the conventional 3D Fourier transform with the combined full k-space dataset.

2.D. Comparison studies and evaluation

The efficacy of the 3D dynamic keyhole imaging with super-resolution (SR_dKeyhole) was compared with zero-filling reconstruction (zero-filled in the k-space data periphery), conventional keyhole reconstruction with low-spatial, high-temporal prior data (LR_cKeyhole), and conventional

keyhole reconstruction with super-resolution prior data (SR_cKeyhole) using MATLAB R2018b (The MathWorks, Natick, USA). All reconstruction techniques used high-spatial resolution central k-space data.

The quality of the reconstructed images with each of four methods was compared with the ground-truth SR images using the original full k-space data. Image quality and artifacts were evaluated using: (a) image intensity difference, (b) structural similarity index (MATLAB function: SSIM),³¹ and (c) average value of image relative error (IRE).¹⁸ SSIM assesses images in terms of luminance, contrast, and structural comparisons; a SSIM value of 1 indicates that the reconstructed image and the original image are identical.

$$IRE = \frac{\sqrt{\sum_{x,y,z} [I_{original}(x,y,z) - I_{recon}(x,y,z)]^2}}{\sqrt{\sum_{x,y,z} [I_{original}(x,y,z)]^2}} \quad (1)$$

where $I_{original}$ is the original image and I_{recon} is the reconstructed image in Eq. (1). An IRE value of 0 indicates that the reconstructed image and the original image are identical.

3. RESULTS

3.A. High-spatial, high-temporal resolution image generation for 3D dynamic keyhole imaging

High-spatial, high-temporal resolution 3D MRI datasets (image matrix: $256 \times 256 \times 10$, spatial resolution: $1.5 \times 1.5 \times 6 \text{ mm}^3$) were generated from low-spatial, high-temporal resolution 3D MRI datasets acquired in the coronal plane (image matrix: $64 \times 64 \times 10$, spatial resolution: $6 \times 6 \times 6 \text{ mm}^3$, acquisition time: 420 ms/volume) by using the cascaded deep learning framework (processing time: <100 ms/volume). Super resolution images were inverse Fourier transformed which were used as high-spatial, high-temporal resolution prior k-space data in 3D dynamic keyhole imaging. Figure 2 shows both the low-spatial resolution (low-spatial resolution: LR) and high-spatial resolution SR (high-spatial resolution: HR) images from four human subjects.

3.B. High-spatial, high-temporal resolution 3D MRI and comparison

Figure 3 shows the high-spatial resolution original image with full k-space data (estimated acquisition time: 1.75 ms/TR \times 256 k_y lines \times 10 k_z lines = 4,480 ms) and the reconstructed high-spatial resolution images of four techniques with the keyhole k-space data (26 k_y lines/slices, estimated acquisition time: 1.75 ms/TR \times 26 k_y lines \times 10 k_z lines = 455 ms). The zero-filling reconstruction resulted in blurred images due to a lack of fine image details from missing peripheral k-space data (zero-filled). The LR_cKeyhole reconstruction resulted in

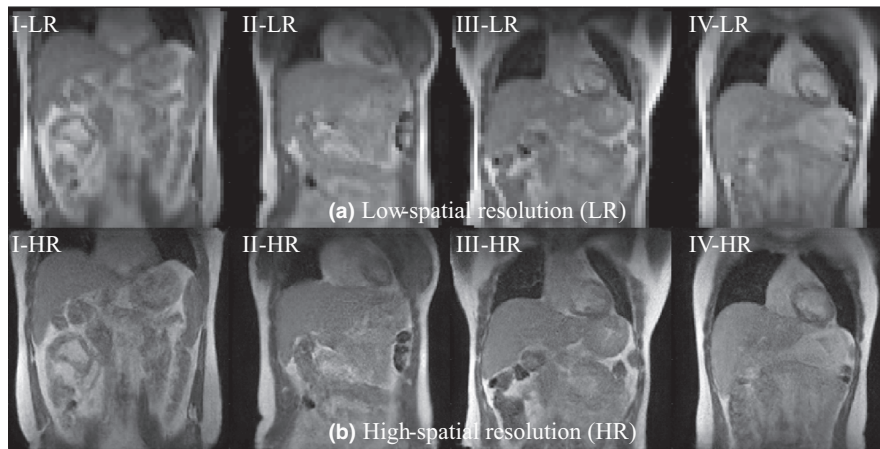


FIG. 2. Top row: (a) Low-spatial resolution (LR) data with image matrix: $64 \times 64 \times 10$, spatial resolution: $6 \times 6 \times 6 \text{ mm}^3$, acquisition time: 420 ms/volume. Bottom row: (b) Output generated from cascaded deep learning framework, high-spatial resolution (HR) data with image matrix: $256 \times 256 \times 10$, spatial resolution: $1.5 \times 1.5 \times 6 \text{ mm}^3$. Generated high-spatial, high-temporal resolution prior images were inverse Fourier transformed which were used in 3D dynamic keyhole imaging. I-VI indicate human subject numbers.

blurred images due to the low-spatial resolution prior data with unmatched motion information. SR_cKeyhole reconstruction improved image quality by using a high-spatial resolution prior dataset, but motion-related artifacts were still present (white arrow) due to utilizing a single prior k-space dataset. SR_dKeyhole reconstructed images were similar to the original SR images since SR_dKeyhole combined high-spatial resolution prior data with motion information. Also, the difference maps of the reconstructed coronal images from the original high-spatial resolution data indicated that SR_dKeyhole was the most favorable technique for real-time high-spatial resolution 3D MRI. The differences of the images are displayed with an intensity range between 0 and 9000 for visual inspection. Structural similarity indices of the reconstructed 3D MRI to the original 3D MRI were 0.65, 0.66, 0.86, and 0.89

for zero-filling, LR_cKeyhole, SR_cKeyhole, and SR_dKeyhole, respectively (1 for identical image). In addition, the IRE scores from comparing the reconstructed 3D MRI to the original 3D MRI were 0.169, 0.191, 0.079, and 0.067 for zero-filling, LR_cKeyhole, SR_cKeyhole, and SR_dKeyhole, respectively.

Figure 4 shows sagittal and axial images of four imaging techniques. Image planes are indicated on the coronal image (s: sagittal imaging plane, ax: axial imaging plane): (a) original SR image, (b) zero-filling image, (c) conventional keyhole image with low-spatial resolution prior data (LR_cKeyhole), (d) conventional keyhole image with super-spatial resolution prior data (SR_cKeyhole), and (e) dynamic keyhole image with super-spatial resolution prior data (SR_dKeyhole), respectively. Since the super-resolution was conducted in the coronal imaging plane, the

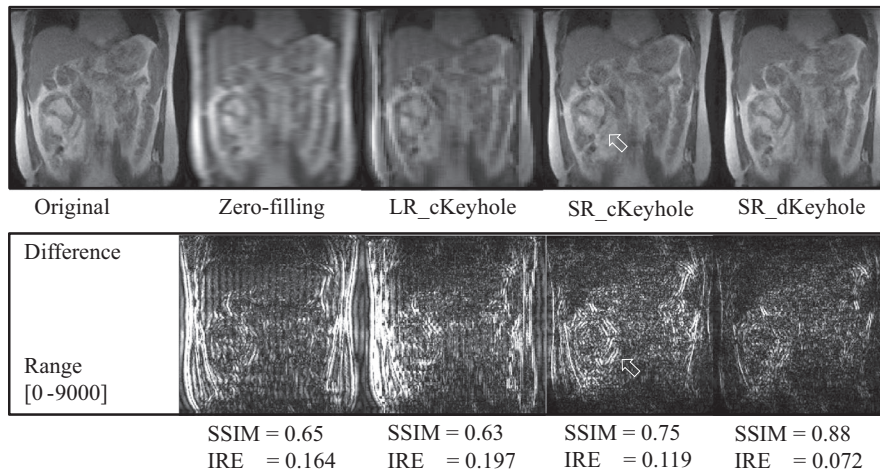


FIG. 3. Comparison of four reconstructed images (estimated acquisition time: 455 ms) to the original image (estimated acquisition time: 4,480 ms): (from left to right) images with full k-space data, zero-filling, conventional keyhole with low-spatial resolution prior data (LR_cKeyhole), conventional keyhole with super-spatial resolution prior data (SR_cKeyhole), and dynamic keyhole with super-spatial resolution prior data (SR_dKeyhole). Top row: Reconstructed coronal images of human subject-I. Bottom row: Image difference between the reconstructed image with the keyhole k-space data and the original image with full k-space data. SSIM: structural similarity index. IRE: average value of image relative error. The white arrow in SR_cKeyhole indicates motion-related artifacts.

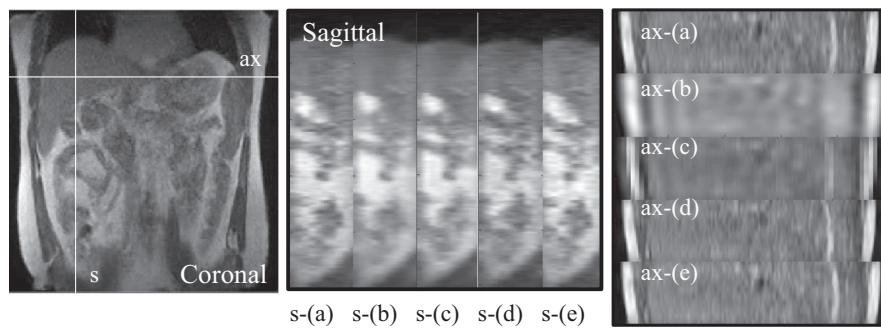


FIG. 4. Sagittal and axial images are presented. Image planes are indicated on the coronal image. (a) Original image, (b) zero-filling, (c) conventional keyhole with low-spatial resolution prior data (LR_cKeyhole), (d) conventional keyhole with super-spatial resolution prior data (SR_cKeyhole), and (e) dynamic keyhole with super-spatial resolution prior data (SR_dKeyhole). s indicates sagittal imaging plane and ax indicates axial imaging plane.

anterior–posterior (AP) direction of the sagittal image and the axial image showed less distinction among four reconstructed images from the original image. According to the visual inspection, SR_dKeyhole reconstructed images were still most similar to the original SR images without any distinct artifacts.

Structural similarity indices are presented in Fig. 5. In the box plot, 37 respiratory samples were included: ten respiratory samples from each human subject I-III and seven respiratory samples from human subject IV (due to long respiratory cycle). Reconstructed 3D images of four human subjects show different level of similarity to the original 3D MRI; SSIM mean \pm SD were 0.65 ± 0.02 , 0.66 ± 0.03 , 0.86 ± 0.07 , and 0.89 ± 0.05 for zero-filling, LR_cKeyhole, SR_cKeyhole, and SR_dKeyhole, respectively. In addition, IRE mean \pm SD were 0.169 ± 0.017 , 0.191 ± 0.025 , 0.079 ± 0.024 , and 0.067 ± 0.016 for zero-filling, LR_cKeyhole, SR_cKeyhole, and SR_dKeyhole, respectively. Reconstructed images by SR_dKeyhole show the highest similarity and the least variance to the original images, while SR_cKeyhole show the second highest similarity but the largest variance to the original images. In contrast, LR_cKeyhole images show the least similarity to the original images.

4. DISCUSSION

In MRgRT, high-spatial volumetric 3D MRI is used for patient alignment and target/organ delineations. During treatment delivery, high-temporal 2D cine MRI (~ 5 frames/sec)² or low-temporal 3D MRI (1 volume/7 s)³ may be used for continuous patient monitoring. However, since tumors near the diaphragm showed 3D motion, both of the approaches cannot properly detect 3D tumor motion in real-time. Therefore, high-spatial, high-temporal resolution 3D MRI is highly needed in real-time MRgRT.

We demonstrated that high-spatial, high-temporal 3D MRI was feasible by combining 3D dynamic keyhole imaging with the SRG model. High-spatial resolution images were prepared as the prior data using super-resolution prior data (<100 ms/volume) generated from low-spatial high-temporal resolution images (<1 min for 20 volumes). 3D dynamic keyhole imaging accelerated the acquisition time by reducing the size of the keyhole data acquired in real-time, resulting in high-temporal resolution imaging. According to our findings, the proposed technique (estimated acquisition time: 455 ms) provided image quality close to the ground-truth SR image with original full k-space data (estimated acquisition time: 4,480 ms). In addition, the proposed technique used the

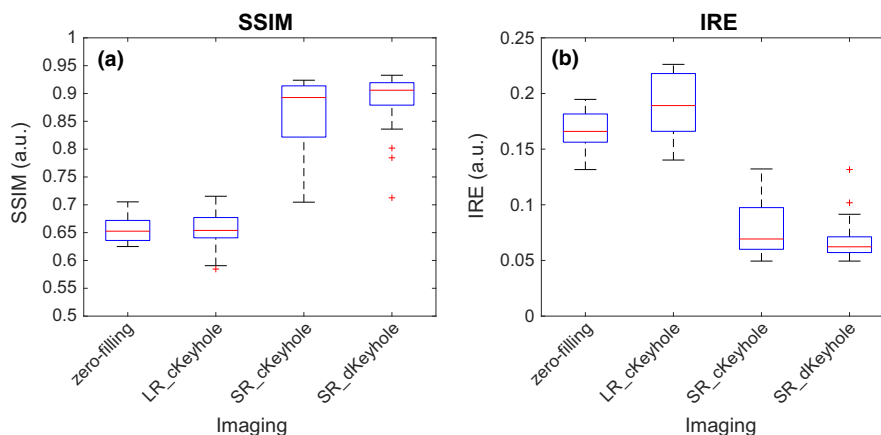


FIG. 5. Box plot of (a) SSIM and (b) IRE in similarity evaluation between the original 3D images and the reconstructed 3D images with four imaging techniques. (a) Mean values of SSIM were 0.65, 0.66, 0.86, and 0.89 for zero-filling, LR_cKeyhole, SR_cKeyhole, and SR_dKeyhole. In addition, (b) mean values of IRE are 0.169, 0.191, 0.079, and 0.067 for zero-filling, LR_cKeyhole, SR_cKeyhole, and SR_dKeyhole, respectively. IRE, image relative error; SSIM, Structural similarity indices. [Color figure can be viewed at wileyonlinelibrary.com]

conventional Fourier transform image reconstruction, so no additional computational time and power were needed, unlike iterative reconstructions of real-time 3D MRI with undersampled schemes and retrospective 4D MRI.^{17–21} Combing parallel, partial Fourier acquisition and/or reduced field of view approaches with 3D dynamic keyhole imaging may further accelerate the 3D MRI imaging time.

In terms of the imaging time, the conventional keyhole imaging with low spatial-resolution prior data (LR_cKeyhole) is feasible without the support of the SRG model. The image quality appears better than the zero-filled reconstructed images. However, SSIM and IRE show that the image similarity of the conventional keyhole images is quite low compared to SR_cKeyhole and SR_dKeyhole, supporting the necessity of high-spatial resolution prior data in keyhole imaging. Also, the SRG model can be directly used to generate high-spatial, high-temporal 3D MRI with higher power computation support. Compared to the direct use of the SRG model, the dynamic keyhole imaging utilized higher input data fidelity, providing a simple and robust imaging method for real-time MRgRT. For example, the SRG model utilizes low-spatial resolution images (image matrix: 64×64 from k-space data matrix with 24 phase encodes using iPAT = 2 and 6/8 partial Fourier). In contrast, the dynamic keyhole reconstruction uses partial high-spatial resolution central k-space data (k-space data matrix: 256×26) in its reconstruction. In addition, the input data fidelity can be increased by updating partial high-spatial resolution peripheral k-space data through temporal data acquisition in the dynamic keyhole imaging. Therefore, higher input data fidelity is a key component of the dynamic keyhole imaging compared to the SRG model approach.

By utilizing anatomical motion information such as respiratory displacement in keyhole imaging, real-time MRI in the presence of respiratory motion can be acquired without substantial motion artifacts. Figures 3 and 5 show the limitation of the conventional keyhole imaging including distinct motion artifacts and similarity variation depending on the respiratory displacement. In Fig. 5, SR_dKeyhole reconstructed images show the highest similarity and the least variance to the original images. SR_cKeyhole show the second highest similarity but the largest variance to the original images due to uncoupling of the prior peripheral k-space data from the temporal central k-space data, thus indicating the importance of the respiratory phase information. In this simulation study, respiratory displacement was extracted from the profile of the diaphragm on the middle coronal slice of the 3D MRI. In MRI scanners, the respiratory signal can be extracted as a 1D Fourier transform of the kx line at the ky-kz center.¹⁸

In our current MRgRT workflow,^{2,3,10} there are no MRI acquisitions occurring between 3D MRI in treatment setup and 2D cine in treatment delivery because there are few treatment preparation steps: patient alignment, daily anatomy-

based delineations, and plan verification. The acquisition dead time can be used for the prior data preparation including the low-spatial, high-temporal imaging (<1 min) and the corresponding SR image generation (<1 min). Once the treatment starts, 3D dynamic keyhole imaging can be launched for real-time 3D MRgRT.

This study has a few limitations. Although four cases showed a promising results based on visual inspection, SSIM and IRE of the reconstructed images, more cases with different levels of motion irregularity may examine the stability of the proposed technique. Second, super-resolution was performed in the coronal imaging plane (in-plane: superior–inferior and left–right) and the through-plane (anterior–posterior) resolution remained (6 mm). The data reduction in 3D dynamic keyhole imaging was only along ky. The data reduction of ky and kz in 3D dynamic keyhole imaging can be studied once the super-resolution conducts in both in-plane and through-plane. Third, the proposed technique has not been tested in the commercial MRIs. All findings were based on off-line simulation. Fourth, 3D image-based segmentation and gating techniques were not studied in this report.

5. CONCLUSION

We demonstrated that high-spatial, high-temporal 3D MRI was feasible by combing 3D dynamic keyhole imaging with the SRG model. The technique's image quality was similar to the original SR images with full k-space data while achieving large accelerations in acquisition time. After the library preparation, there was no additional computational time and power needed with the conventional Fourier transform image reconstruction in 3D imaging unlike undersampled approaches. Validating and evaluating robustness of the technique are ongoing. Based on our findings, the proposed 3D dynamic keyhole imaging combined with the SRG model is a promising technique for real-time MRgRT, which will establish a paradigm for real-time 3D imaging scheme, structure segmentation, and gating algorithm.

ACKNOWLEDGMENTS

Provisional patent “Methods and Systems for Real-Time 3D MRI” on file. Dr. Mutic has consulted for ViewRay and Varian. Washington University in St. Louis has a master research agreement and receives research funding from ViewRay unrelated to this study.

CONFLICT OF INTEREST

The authors have no relevant conflicts of interest to disclose.

^{a)}Author to whom correspondence should be addressed. Electronic mail: taehokim@wustl.edu; Telephone: +314-273-3316.

REFERENCES

- Mutic S, Dempsey JF. The ViewRay system: magnetic resonance-guided and controlled radiotherapy. *Semin Radiat Oncol*. 2014;24:196–199.
- Green OL, Rankine LJ, Cai B, et al. First clinical implementation of real-time, real anatomy tracking and radiation beam control. *Med Phys*. 2018;45:3728–3740.
- Raaymakers B, Jürgenliemk-Schulz I, Bol G, et al. First patients treated with a 1.5 T MRI-Linac: clinical proof of concept of a high-precision, high-field MRI guided radiotherapy treatment. *Phys Med Biol*. 2017;62:L41–L50.
- Henke L, Contreras J, Green O, et al. Magnetic resonance image-guided radiotherapy (MRIgRT): A 4.5-year clinical experience. *Clin Oncol (R Coll Radiol)*. 2018;30:720–727.
- Jia X, Tian Z, Xi Y, Jiang SB, Wang G. New concept on an integrated interior magnetic resonance imaging and medical linear accelerator system for radiation therapy. *J Med Imaging*. 2017;4:015004.
- Keall PJ, Barton M, Crozier S. The Australian magnetic resonance imaging–linac program. *Semin Radiat Oncol*. 2014;24:203–206.
- Fallone B, Murray B, Rathee S, et al. MR images obtained during megavoltage photon irradiation from a prototype integrated linac-MR system. *Med Phys*. 2009;36:2084–2088.
- Liney GP, Whelan B, Oborn B, Barton M, Keall P. MRI-linear accelerator radiotherapy systems. *Clin Oncol (R Coll Radiol)*. 2018;30:686–691.
- de Koste JRvS, Palacios MA, Bruynzeel AM, Slotman BJ, Senan S, Lagerwaard FJ. MR-guided gated stereotactic radiation therapy delivery for lung, adrenal, and pancreatic tumors: a geometric analysis. *Int J Radiat Oncol Biol Phys*. 2018;102:858–866.
- Werensteijn-Honingh AM, Kroon PS, Winkel D, et al. Feasibility of stereotactic radiotherapy using a 1.5 T MR-linac: Multi-fraction treatment of pelvic lymph node oligometastases. *Radiother Oncol*. 2019;134:50–54.
- Heerkens HD, Van Vulpen M, Erickson B, et al. MRI guided stereotactic radiotherapy for locally advanced pancreatic cancer. *British J Radiol*. 2018;91:20170563.
- Henke LE, Green OL, Schiff J, et al. First Reported Case of Pediatric Radiation Treatment with Magnetic Resonance Image-Guided Radiotherapy. *Advances in Radiation Oncology*. 2019;31:233–236.
- Stemkens B, Paulson ES, Tijssen RH. Nuts and bolts of 4D-MRI for radiotherapy. *Phys Med Biol*. 2018;63:21TR01.
- Lee D, Kim S, Palta J, Keall BL, Kim T. A retrospective 4D-MRI based on 2D diaphragm profiles for lung cancer patients. *J Med Imaging Radiat Oncol*. 2019;63:360–369.
- Harris W, Yin F-F, Wang C, Zhang Y, Cai J, Ren L. Accelerating volumetric cine MRI (VC-MRI) using undersampling for real-time 3D target localization/tracking in radiation therapy: a feasibility study. *Phys Med Biol*. 2017;63:01NT01.
- Lee D, Greer PB, Ludbrook J, et al. Audiovisual biofeedback improves cine-magnetic resonance imaging measured lung tumor motion consistency. *Int J Radiat Oncol Biol Phys*. 2016;94:628–636.
- Han F, Zhou Z, Cao M, Yang Y, Sheng K, Hu P. Respiratory motion-resolved, self-gated 4D-MRI using rotating cartesian k-space (ROCK). *Med Phys*. 2017;44:1359–1368.
- Wang C, Subashi E, Yin F-F, Chang Z, Cai J. A Spatiotemporal-Constrained Sorting Method for Motion-Robust 4D-MRI: a feasibility study. *Int J Radiat Oncol Biol Phys*. 2019;103:758–766.
- Deng Z, Pang J, Yang W, et al. Four-dimensional MRI using three-dimensional radial sampling with respiratory self-gating to characterize temporal phase-resolved respiratory motion in the abdomen. *Magn Reson Med*. 2016;75:1574–1585.
- Kim YC, Lebel RM, Wu Z, Ward SLD, Khoo MC, Nayak KS. Real-time 3D magnetic resonance imaging of the pharyngeal airway in sleep apnea. *Magn Reson Med*. 2014;71:1501–1510.
- Uecker M, Zhang S, Voit D, Dietmar K, Frahm J. Real-time MRI: recent advances using radial FLASH. *Imaging Med*. 2012;4:461–476.
- Suh Y, Dieterich S, Cho B, Keall PJ. An analysis of thoracic and abdominal tumour motion for stereotactic body radiotherapy patients. *Phys Med Biol*. 2008;53:3623.
- Plathow C, Schoebinger M, Fink C, et al. Quantification of lung tumor volume and rotation at 3D dynamic parallel MR imaging with view sharing: preliminary results. *Radiology*. 2006;240:537–545.
- Keall PJ, Mageras GS, Balter JM, et al. The management of respiratory motion in radiation oncology report of AAPM Task Group 76a. *Med Phys*. 2006;33:3874–3900.
- Van Vaals JJ, Brummer ME, Thomas Dixon W, et al. “Keyhole” method for accelerating imaging of contrast agent uptake. *J Magn Reson Imaging*. 1993;3:671–675.
- Lee D, Greer PB, Pollock S, Kim T, Keall P. Quantifying the accuracy of the tumor motion and area as a function of acceleration factor for the simulation of the dynamic keyhole magnetic resonance imaging method. *Med Phys*. 2016;43:2639–2648.
- Lee D, Pollock S, Whelan B, Keall P, Kim T. Dynamic keyhole: A novel method to improve MR images in the presence of respiratory motion for real-time MRI. *Med Phys*. 2014;41:072304.
- Van Reeth E, Tham IW, Tan CH, Poh CL. Super-resolution in magnetic resonance imaging: a review. *Concepts Mag Reson Part A*. 2012;40:306–325.
- Chun J, Zhang H, Gach HM, et al. MRI super resolution reconstruction for MRI-guided adaptive radiotherapy using cascaded deep learning: in the presence of limited training data and unknown translation model. *Medical physics*. 2019;46:4148–4164.
- Manjón JV, Coupé P, Buades A, Fonov V, Collins DL, Robles M. Non-local MRI upsampling. *Med Image Anal*. 2010;14:784–792.
- Wang Z, Bovik AC, Sheikh HR, Simoncelli EP. Image quality assessment: from error visibility to structural similarity. *IEEE Trans Image Process*. 2004;13:600–612.